

Streamlined Darwin Simulation of Nonneutral Plasmas

DENNIS W. HEWETT AND JOHN K. BOYD

Lawrence Livermore National Laboratory, Livermore, California 94550

Received April 18, 1986; revised August 22, 1986

Efficient, new algorithms that require less formal manipulation than previous implementations have been formulated for the numerical solution of the Darwin model. These new procedures reduce the effort required to achieve some of the advantages that the Darwin model offers. Because the Courant-Friedrichs-Lewy stability limit for radiation modes is eliminated, the Darwin model has the advantage of a substantially larger time-step. Further, without radiation modes, simulation results are less sensitive to enhanced particle fluctuation noise. We discuss methods for calculating the magnetic field that avoid formal vector decomposition and offer a new procedure for finding the inductive electric field. This procedure avoids vector decomposition of plasma source terms and circumvents some source gradient issues that slow convergence. As a consequence, the numerical effort required for each of the field time-steps is reduced, and more importantly, the need to specify several nonintuitive boundary conditions is eliminated. © 1987 Academic Press, Inc.

I. INTRODUCTION

It is frequently useful to simulate low-frequency electromagnetic (EM) plasma phenomena without time resolution of purely EM modes. The Darwin or magnetoinductive limit [1-5] of Maxwell's equations provides a model that neglects retardation effects and therefore neglects plasma source coupling to purely EM modes. Many nonneutral EM models can be constructed that neglect radiation; however, the Darwin model accomplishes the radiationless limit while retaining the correct particle Lagrangian through terms of order v^2/c^2 . This is a higher order than other models in common use. In addition, the Darwin model retains that part of the displacement current necessary for the charge continuity equation to be satisfied. In the field solution for nonneutral plasma models this is especially important.

Darwin simulation models have at least two numerical advantages over fully EM

models. First, the Darwin model eliminates the rather restrictive CFL condition [6] on the time step. Roughly, this condition is a stability constraint such that light cannot propagate more than the minimum computational cell dimension in a time step. A second advantage, pointed out by Nielson and Lewis [2], is that the Darwin model provides relief from “excessive bremsstrahlung.” Particle representations of plasmas exhibit anomalously large fluctuations resulting from the relatively small ratio of simulation to real particles. These fluctuations drive much more than realistic amounts of energy into purely EM modes. Thus, full EM codes require more particles per simulation cell than Darwin model codes to control these fluctuation levels.

A disadvantage of the Darwin model is that the field solution is more complex than the full EM models. The full set of Maxwell’s equations are hyperbolic in character and lend themselves to straightforward leapfrog schemes in which \mathbf{E} and \mathbf{B} are advanced in time with a simple sweep over the mesh. The Darwin limit of Maxwell’s equations is a system of field equations that has instantaneous propagation of fields throughout the system given the instantaneous source terms. Although the Darwin field solution needs to be carried out fewer times because of the larger Δt , each field solve requires more work to propagate the field changes due to source and induction terms throughout the mesh. Careful numerical implementation and rapid elliptic solution techniques are required to achieve full benefit of the model. In particular, the elliptic solution methods need to be global so that information is propagated across the mesh quickly. A Darwin field solution using point relaxation methods can take more effort than subcycling the fully EM hyperbolic model.

A straightforward implementation of the Darwin model (hereafter referred to as the “standard” method) requires vector decomposition of some plasma source terms into irrotational and solenoidal parts. As will be discussed, the standard method seems to necessitate vector decomposition of source terms as well as “divergence cleaning” (the process of decomposing a vector and discarding its irrotational part) inside iteration loops for the solution of the inductive part of the electric field.

A more difficult problem is that boundary conditions must be specified for these vector decompositions for which no source of intuition is readily available. As more general boundary conditions are required to properly represent the physics, the interrelatedness of these conditions increases. In Fig. 1 we give a representative example of a simulation region with complicated boundaries that motivated our search for more intuitive techniques. This example comes from an axisymmetric $r-z$ Darwin simulation of an electron gun with internal cathode–anode placement [7]. We have recently found ways to avoid many of the most challenging boundary conditions. The purpose of this paper is to present a way of eliminating or streamlining some of this “extra” work while still retaining all the properties of the original Darwin limit. The Darwin limit of Maxwell’s equations is given in Section II. In Section III a new streamlined prescription for accomplishing the Darwin solution is presented. Test cases verifying the new streamlined method are given in Section IV.

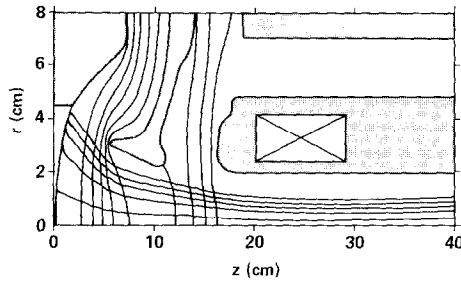


FIG. 1. A representative example of a simulation region with complicated internal boundaries that motivated our search for techniques that do not require decomposition of the plasma source terms \mathbf{J} and $\dot{\mathbf{J}}$. This example comes from an axisymmetric $r-z$ Darwin simulation of an electron gun with internal cathode-anode placement.

II. THE DARWIN MODEL

The essence of the Darwin model is to neglect only the inductive or solenoidal part (denoted by subscript t) of the displacement current. The resulting field equations are

$$\nabla \times \mathbf{B} = 4\pi/c \mathbf{J}_t, \quad (1a)$$

$$\nabla \cdot \mathbf{B} = 0, \quad (1b)$$

$$\nabla \times \nabla \times \mathbf{E} = -4\pi/c^2 \dot{\mathbf{J}}_t, \quad (1c)$$

$$\nabla \cdot \mathbf{E} = 4\pi\rho \quad (1d)$$

in which \mathbf{E} and \mathbf{B} are the electric and magnetic fields and ρ and \mathbf{J} are the plasma source terms that are obtained by integrating over the ensemble of moving point charges. We have used a combination of Gauss's law and the charge continuity equation to obtain $\mathbf{J}_t = \mathbf{J} + \dot{\mathbf{E}}_t/c$. A derivation of the model can be found in Nielson and Lewis [2].

A straightforward implementation of these equations requires vector decomposition into irrotational (denoted by subscript l) and solenoidal parts. Our prescription for the decomposition of a general vector field \mathbf{G} is accomplished by writing that vector field as the sum of irrotational and solenoidal vectors,

$$\mathbf{G} = \mathbf{G}_l + \mathbf{G}_t, \quad (2a)$$

where

$$\mathbf{G}_l = -\nabla\psi. \quad (2b)$$

Taking the divergence of Eq. (2a) yields the Poisson equation

$$\nabla^2\psi = -\nabla \cdot \mathbf{G}. \quad (2c)$$

Solving for ψ with appropriate boundary conditions provides the irrotational part \mathbf{G}_i using Eq. (2b). The solenoidal part is obtained by subtracting \mathbf{G}_i from the original vector

$$\mathbf{G}_s = \mathbf{G} - \mathbf{G}_i = \mathbf{G} + \nabla\psi. \quad (2d)$$

The boundary conditions required for Eq. (2c) can be devised from the mathematical requirement of specifying the normal component of \mathbf{G}_i ($= -\nabla\psi$) on the simulation boundaries. It can be shown that a decomposition according to these rules is unique [8, 9]. We take this procedure as our definition of the irrotational and solenoidal decomposition of a vector field.

The Darwin limit of Maxwell's equations require decomposition \mathbf{J} and $\dot{\mathbf{J}}$, necessitating specification of the normal components of \mathbf{J}_i and $\dot{\mathbf{J}}_i$. In addition, practical solutions of this set of equations require divergence cleaning of \mathbf{B} in the solution of Eq. (1a) as well as \mathbf{E}_i in the solution of Eq. (1c). Boundary conditions are needed on all simulation boundaries for each of these decompositions. Many of these choices require intuition about quantities whose properties are unfamiliar because of their remote connection to physical variables. With nonneutral plasmas that have significant charge and current densities near internal conductors, developing a useful Darwin model can be very challenging.

III. STREAMLINED SOLUTION METHODS

Several techniques have been developed for eliminating some of the formal manipulation that seems to be required by the standard solution of the Darwin model. The main point of our streamlined method is that decomposition of source terms can be eliminated, thus avoiding the specification of boundary conditions for quantities for which intuition is weak. Another benefit is the reduction in computation—especially important for iterative solutions. We have devised a streamlined \mathbf{E}_i iteration procedure that provides the solution without formal source decomposition. We first discuss the \mathbf{B} calculation because \mathbf{B} is needed in the source for the \mathbf{E}_i calculation and the principles for avoiding decomposition can be cogently introduced without the complication of iteration.

III.a. Streamlined \mathbf{B} Solution

In general, there are two methods of solving for \mathbf{B} : the first method solves for the magnetic vector potential \mathbf{A} and obtains \mathbf{B} by taking the curl of \mathbf{A} . This method ensures \mathbf{B} is purely solenoidal. For this method the magnetic field solution is streamlined by avoiding decomposition of the current source term, noting that spurious values of \mathbf{A}_i do not contribute to \mathbf{B} . In the second method we solve for \mathbf{B} directly. In this method it is not necessary to decompose the source although boundary conditions must be carefully chosen to guarantee $\nabla \cdot \mathbf{B} = 0$. This method is streamlined in the sense that source decomposition is eliminated by a curl

operation. Both methods are presented, since their usage is dependent on the particular physics that is being studied. For example, in the case of a theta pinch with a voltage specified at a boundary, it is most natural to work with the vector potential. The voltage for this case is easily entered as the time derivative of the tangential components of \mathbf{A} .

In the first method, we replace \mathbf{B} in Eqs. (1a), (1b) by

$$\mathbf{B} = \nabla \times \mathbf{A}. \quad (3)$$

This choice ensures $\nabla \cdot \mathbf{B} = 0$ since $\nabla \cdot (\nabla \times \mathbf{A}) = 0$. Substituting Eq. (3) into Eq. (1a), we have the governing equation

$$\nabla \times \nabla \times \mathbf{A} = 4\pi/c \mathbf{J}_t \quad (4)$$

which becomes

$$\nabla^2 \mathbf{A} = -4\pi/c \mathbf{J}_t \quad (5)$$

in the Coulomb gauge using the vector identity

$$\nabla^2 \mathbf{G} = \nabla(\nabla \cdot \mathbf{G}) - \nabla \times \nabla \times \mathbf{G}, \quad (6)$$

assuming that we have accumulated the total current \mathbf{J} from the plasma time advance. The standard solution of Eq. (5) is to first decompose \mathbf{J} using Eqs. (2c), (2d) with boundary conditions for (2c) that involve specifying the normal component of \mathbf{J}_t ($= \hat{\mathbf{n}} \cdot \nabla \psi$) on all boundaries. Generally, physics rationale for this boundary condition can be based on conditions used for the \mathbf{E} calculation: the normal component $\hat{\mathbf{n}} \cdot \mathbf{E}$ can be related to the emitted normal current.

As we have already stated, the standard procedure just described involves more work than necessary. If we fail to adequately decompose \mathbf{J} in steps (2c), (2d), \mathbf{J}_t will have an irrotational part. Since vector decomposition is unique, we must then have

$$\nabla(\nabla \cdot \mathbf{A}) = -4\pi/c \mathbf{J}_t \neq 0, \quad (7)$$

which violates the Coulomb gauge condition in the interior of the mesh. Fortunately, \mathbf{B} as given by Eq. (3) is invariant to this error—leading us to the streamlined approach. Obviously, there is no penalty for doing a *very* poor job of finding \mathbf{J}_t from \mathbf{J} , so we may dispense with the decomposition step altogether. We solve

$$\nabla^2 \mathbf{A} = -4\pi/c \mathbf{J} \quad (8)$$

directly and then extract \mathbf{B} by application of Eq. (3).

Note that in eliminating the decomposition we have also obviated the boundary conditions associated with the Poisson solution that Eq. (2c) needed to decompose \mathbf{J} . Boundary conditions required for Eq. (8) are the same as used in the standard method in Eq. (5).

The second method avoids the divergence-clean of \mathbf{J} by taking the curl of

Eq. (1a) directly. This method is suitable in cases where \mathbf{B} boundary conditions are readily available. The curl of Eq. (1a) gives

$$\nabla \times \nabla \times \mathbf{B} = 4\pi/c \nabla \times \mathbf{J}_t, \quad (9)$$

which eliminates the decomposition of \mathbf{J} , since $\nabla \times \mathbf{J} = \nabla \times \mathbf{J}_t$. Using Eq. (6), we find the vector \mathbf{B} by solving

$$\nabla^2 \mathbf{B} = -4\pi/c \nabla \times \mathbf{J} \quad (10)$$

using boundary conditions that require $\nabla \cdot \mathbf{B} = 0$ on the boundary. For example, with Cartesian geometry and B_y Dirichlet condition $B_y(x=0, y)$, the appropriate B_x boundary condition is the Neumann condition $\partial B_x / \partial x = -\partial B_y / \partial y$ at $x=0$. We obtain from the solution of Eq. (10) a vector \mathbf{B} that satisfies Eq. (9) and, in addition, satisfies

$$\nabla^2 \mathbf{B} = \nabla(\nabla \cdot \mathbf{B}) = 0 \quad (11)$$

which implies $\nabla \cdot \mathbf{B} = 0$ everywhere.

For completeness, a combination of these two methods, useful in two dimensions, eliminates decomposition by introducing a flux function equation. The flux function is simply proportional to the component of the magnetic vector potential normal to the two-dimensional plane of interest. The equation to be solved is then the normal component of Eq. (5). No decomposition is necessary because, in two dimensions, $\mathbf{J}_{\text{normal}}$ must be purely solenoidal; the normal component can have no gradient contribution by definition. The curl of this flux function provides both components of \mathbf{B} in the computational plane. The normal component $\mathbf{B}_{\text{normal}}$ completes the magnetic field description and may be computed from the curl of Eq. (1a) directly. The equation is

$$\nabla^2 \mathbf{B}_{\text{normal}} = -4\pi/c [\nabla \times \mathbf{J}]_{\text{normal}}. \quad (12)$$

III.b. Streamlined \mathbf{E} Solution

The total electric field \mathbf{E} can be written as the sum of the inductive or solenoidal part \mathbf{E}_i and the electrostatic or irrotational part \mathbf{E}_t , which can be derived from the electrostatic potential Φ . Writing this sum as $\mathbf{E} = \mathbf{E}_i - \nabla\Phi$ and substituting into Eq. (1d), we get Poisson's equation

$$\nabla^2 \Phi = -4\pi\rho \quad (13)$$

for the irrotational electric field, where ρ is the charge density.

The equation for \mathbf{E}_t in Darwin simulation models requires developing an implicit representation for \mathbf{J} . In previous work [2, 4], \mathbf{J} has been obtained by adding the momentum equations for each species so that Eq. (1c) can be written

$$\nabla^2 \mathbf{E}_t = 4\pi/c^2 \mathbf{J}_t = 4\pi/c^2 [\mathbf{D} + \mu(\mathbf{E}_i + \mathbf{E}_t) + \zeta \times \mathbf{B}]_t, \quad (14)$$

where \mathbf{D} represents divergence of the kinetic energy tensors, μ is the sum of the plasma frequencies, and ζ is the corresponding quantity associated with the currents [4].

To motivate the streamlined procedure for solving Eq. (14), we first review the standard Darwin solution procedure. Since the right-hand side of Eq. (14) explicitly contains \mathbf{E}_i in an expression that must be vector decomposed, iteration (denoted by the superscript n) will be required to obtain a consistent solution. A straightforward algorithm used previously for the standard method is:

(1) Form \mathbf{J} using the latest \mathbf{E}_i^n and vector-decompose to find \mathbf{J}_i using Eq. (2c) and (2b).

(This requires specifying the normal component of \mathbf{J}_i on the boundaries.)

(2) Solve

$$\nabla^2 \mathbf{E}_i^{n+1} = 4\pi/c^2 \mathbf{J}_i^n. \quad (15)$$

(Boundary conditions must ensure that $\mathbf{V} \cdot \mathbf{E}_i = 0$ on the boundaries.)

(3) Divergence-clean \mathbf{E}_i^{n+1} using Eq. (2c) and (2b) to eliminate any spurious irrotational part due to imperfect decomposition of \mathbf{J} in step (1).

(4) Set n equal to $n+1$; check convergence; if not converged, go to step (1).

(5) Add \mathbf{E}_i^n and \mathbf{E}_i to get the final \mathbf{E} .

The decomposition in step (3) is required to ensure \mathbf{E}_i does not develop an irrotational part as the iteration progresses should the \mathbf{J}_i from step (1) not be purely solenoidal. Furthermore, finite mesh considerations in the solution of Eq. (15) also require divergence cleaning to avoid growth of any spurious irrotational part of \mathbf{E}_i . A straightforward boundary condition for this step is that the normal gradient of ψ (which is $-(\mathbf{E}_i)_i \cdot \hat{n}$) be set to $\mathbf{E}_i \cdot \hat{n}$ —assuming that we wish to have the divergence-cleaned \mathbf{E}_i have a zero normal component everywhere. More general boundary conditions can be difficult to implement; we defer this discussion until our streamlined procedure has been introduced.

Assuming acceptable solutions for the boundary condition issues, the five-step standard procedure just outlined may converge slowly and is quite expensive due to the number of elliptic solutions required in each iteration. Convergence can be substantially enhanced with the addition of the explicit term $\mu \mathbf{E}_i$ to each side [2]. Equation (14) then becomes

$$\nabla^2 \mathbf{E}_i^{n+1} - 4\pi/c^2 \mu \mathbf{E}_i^{n+1} = 4\pi/c^2 (\mathbf{J}_i^n - \mu \mathbf{E}_i^n). \quad (16)$$

The additional term is most important when μ is nearly constant in space so that $\mu \mathbf{E}_i$ is roughly equal to $(\mu \mathbf{E}_i)_i$ —the term embedded in \mathbf{J}_i . In this case the right-hand side of Eq. (16) becomes independent of \mathbf{E}_i . The addition loses effectiveness as the density becomes strongly inhomogeneous. A side effect of this additional term is that an irrotational piece of \mathbf{E}_i may develop during the overall iteration satisfying

part when using Eq. (10).

We propose a streamlined algorithm for the solenoidal \mathbf{E} calculation that provides substantial improvements over the standard implementation just presented. In practice, the source which is readily available is \mathbf{J} , *not* the solenoidal part \mathbf{J}_s . Our improvements result largely from a better iteration procedure that does not require a *formal* decomposition of the right-hand side of Eq. (14), thus obviating the most difficult boundary issues concerning $\mathbf{J}_s \cdot \hat{n}$. The fundamental strategy of the streamlined method is to solve an equation for \mathbf{E}_t with the total \mathbf{J} as the source. This strategy is similar to the first \mathbf{B} solution in Section III.a except that we cannot ignore the spurious irrotational part of \mathbf{E}_t . We must ensure $\nabla \cdot \mathbf{E}_t = 0$ and, therefore, we add an additional irrotational part to Eq. (14) that compensates for the use of the entire \mathbf{J} ,

$$\nabla^2 \mathbf{E}_t - \nabla^2 (\nabla \psi) = 4\pi/c^2 \mathbf{J}. \quad (17)$$

Defining the variable $\xi = \mathbf{E}_t - \nabla \psi$, Eq. (17) becomes

$$\nabla^2 \xi = 4\pi/c^2 \mathbf{J}. \quad (18)$$

The irrotational part of Eq. (17) is an elliptic equation for $\nabla \psi$ with source $(4\pi/c^2) \mathbf{J}_s$. A unique solution to this equation could be obtained by specifying a boundary condition for $\nabla \psi$. Thus, by superposition a consistent boundary condition for Eq. (18) is found by specifying the given \mathbf{E}_t boundary condition modified by a contribution from ψ . Before presenting this modification, we first consider the boundary conditions we require \mathbf{E}_t to satisfy.

A well-posed formulation for the solution of Eq. (14) for \mathbf{E}_t requires specification of either Dirichlet or Neumann boundary conditions on all boundaries. The choice of these boundary conditions must be consistent with $\nabla \cdot \mathbf{E}_t = 0$. We choose to specify \mathbf{E}_t tangential and then infer boundary conditions on normal components from $\nabla \cdot \mathbf{E}_t = 0$. For example, in a Cartesian region a Dirichlet boundary specification of E_{tx} on a horizontal boundary implies the Neumann condition $\partial E_{ty} / \partial y = -\partial E_{tx} / \partial x$ on that horizontal boundary for the E_{ty} equation. This is similar in spirit to guaranteeing $\nabla \cdot \mathbf{B} = 0$ as discussed in Section III.a for the magnetic field solution.

Now we consider how these conditions are reflected in the boundary conditions for ξ in Eq. (18). In the case of a Dirichlet boundary condition for the \mathbf{E}_t solution, we use

$$\xi(b) = \mathbf{E}_t(b) - \nabla \psi(b). \quad (19)$$

where the argument b signifies evaluation on the boundary. In the case of a Neumann boundary condition in the \mathbf{E}_t solution, we use the normal derivative of Eq. (19). Neither of these conditions can be applied without knowing the properties of ψ on the boundary.

The equation for ψ is obtained from the divergence of the defining relation for ξ which is

$$\nabla^2\psi = -\nabla \cdot \xi. \quad (20)$$

The boundary condition for Eq. (20) can simply be Dirichlet zero for ψ because whatever $\nabla\psi$ may be, the boundary value is communicated through Eq. (19) to Eq. (18). Similarly for the Neumann condition, the normal derivative of $\nabla\psi$ on the boundary is communicated through the normal derivative of Eq. (19) to Eq. (18). Upon solving Eq. (20), we immediately have the required boundary condition needed to solve Eq. (18). Technically, Eqs. (18) and (20) must be solved simultaneously, but in practice iteration over these equations has been sufficient.

Since the right-hand side of Eq. (16) does not need to be formed and then divergence-cleaned, we can move the \mathbf{E}_t term in \mathbf{J} to the left-hand side to speed convergence. Displaying explicitly the functional dependences, we have

$$\nabla^2\xi^{n+1} - 4\pi/c^2 \mu\xi^{n+1} = 4\pi/c^2[\mathbf{D} + \mu\mathbf{E}_t + \zeta \times \mathbf{B} + \mu \nabla\psi^n], \quad (21)$$

where $\xi_t = -\nabla\psi$ and iteration has been introduced with the superscript n . At convergence, we have

$$\nabla^2\xi - 4\pi/c^2 \mu\xi_t = 4\pi/c^2[\mathbf{D} + \mu\mathbf{E}_t + \zeta \times \mathbf{B}]. \quad (22)$$

The streamlined solution procedure for ξ consists of the following steps:

- (1) Solve Eq. (21) for ξ^{n+1} using appropriate boundary conditions and the most recent ψ .
- (2) Check convergence of ξ^{n+1} ; if converged, go to step (4).
- (3) Find ψ^{n+1} —the first step of a ξ^{n+1} decomposition—using

$$\nabla^2\psi^{n+1} = -\nabla \cdot \xi^{n+1} \quad (23)$$

with Dirichlet $\psi = 0$ boundary conditions. Set n equal to $n + 1$; go to step (1).

- (4) Add \mathbf{E}_t^{n+1} ($= \xi + \nabla\psi^{n+1}$) and \mathbf{E}_t to get the final \mathbf{E} .

As previously discussed, the appropriate boundary conditions to ensure that the solution of Eq. (22) will contain the desired \mathbf{E}_t are needed for steps (1) and (3) and are relatively easy to apply. The normal component of ξ_t ($= -\nabla\psi$) is automatically incorporated without any user input. Further, note if $\nabla \cdot \xi = 0$, then the solution of Eq. (23) with Dirichlet boundary conditions gives $\psi = 0$ everywhere. Thus, ψ is seen to be the scalar function that precisely compensates for the longitudinal part of \mathbf{J} in Eq. (17).

The boundary conditions needed for the iterative solution of Eq. (21) can now be explicitly stated. For a given component of Eq. (21), we choose Dirichlet boundary conditions $\mathbf{E}_t(b)|_{\text{tan}}$ on those boundaries that are tangential to that component.

(We use the subscripts tan and nor to signify the tangential and normal components, respectively.) This condition on $\mathbf{E}_t|_{\text{tan}}$ in terms of $\xi(b)|_{\text{tan}}$ is

$$\xi(b)|_{\text{tan}} = \mathbf{E}_t(b)|_{\text{tan}} - \nabla\psi''(b)|_{\text{tan}}. \quad (24)$$

For the normal component of Eq. (21) on this same boundary, there is no freedom in the normal derivative of ξ if it is to be consistent with $\mathbf{V} \cdot \mathbf{E}_t(b) = 0$. Requiring the divergence to be zero on the boundary leads to the Neumann condition

$$\partial_{\text{nor}}[\mathbf{E}_t(b)|_{\text{nor}}] = -\partial_{\text{tan}}[\mathbf{E}_t(b)|_{\text{tan}}] \quad (25)$$

which, using $\mathbf{E}_t = \xi + \nabla\psi$, can be written

$$\partial_{\text{nor}}[\xi^{n+1}(b)|_{\text{nor}}] = -\partial_{\text{tan}}[\mathbf{E}_t(b)|_{\text{tan}}] - \partial_{\text{nor}}^2\psi''(b). \quad (26)$$

Finally, if ψ is a constant along the boundary, its derivative along the boundary vanishes, and using Eq. (20), the condition reduces to

$$\partial_{\text{nor}}[\xi^{n+1}(b)|_{\text{nor}}] = -\partial_{\text{tan}}[\mathbf{E}_t(b)|_{\text{tan}}] + \mathbf{V} \cdot \xi''(b). \quad (27)$$

These boundary constraints, coupled with the last application of step (5), completes the solution for \mathbf{E}_t . The streamlined method obviates the specification of $\xi_t \cdot \hat{n}$ on the boundaries—the usual difficulty with step (3).

Finally, we emphasize again that since \mathbf{J} no longer needs to be decomposed in the streamlined method, we are spared the difficulty of specifying boundary conditions on $\mathbf{J}_t \cdot \hat{n}$, which are required in the standard method.

IV. TEST CASES

We now present a series of tests that verify the new streamlined Darwin methods produce the correct fields. Numerical implementation of either the standard or streamlined model requires the ability to decompose vectors with some degree of accuracy. Ideally, a divergence-cleaned vector will in fact produce a satisfactory zero when subjected to the numerical divergence operation. The most convenient way to guarantee this behavior is to use a suitably interleaved mesh such that $\mathbf{V} \cdot \mathbf{V}\Phi = 0$. To test the concepts presented here, it is sufficient to use a less precise cell-centered mesh. The discrete grid implemented in our test code is given by

$$X_i = X_{\min} + (i - 1.5)(X_{\max} - X_{\min})/N_x = X_{\min} + (i - 1.5)\Delta x, \quad (28a)$$

$$Y_j = Y_{\min} + (j - 1.5)(Y_{\max} - Y_{\min})/N_y = Y_{\min} + (j - 1.5)\Delta y. \quad (28b)$$

We simplify our problem further by allowing arbitrary boundary conditions on the x boundaries but let the system be periodic in the y direction. We use $X_{\min} = Y_{\min} = 0$, $X_{\max} = Y_{\max} = 20$, and $N_x = N_y = 42$ in the examples presented here.

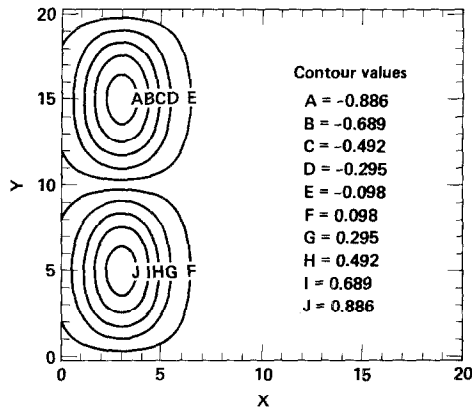


FIG. 2. Contours of constant J_z used as the input current for the **B** calculation test.

B Tests

The direct **B** solution is tested to demonstrate the ability to solve for a zero-divergence magnetic field. This test also shows a practical example of successfully applying boundary conditions consistent with zero divergence. The effect of this requirement has been much easier to study in the direct **B** solution where interrelated numerical iteration issues are not present.

To initialize the direct **B** calculation, we select an arbitrary current directed out of the $X - Y$ mesh. We take for this test the form

$$J_z(i, j) = \exp\{-[X(i) - a]^2/5\} \sin[\pi Y(j)/10]. \tag{29}$$

A contour plot of this function is given in Fig. 2, where $a = 3$. Taking the curl of J_z gives the vector components needed for the right-hand side of Eq. (10). These components are shown in the $x - y$ plane by the vector plot in Fig. 3. We have

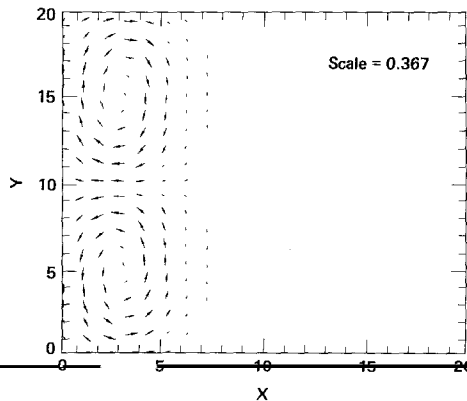


FIG. 3. The curl of J_z shown in Fig. 2.

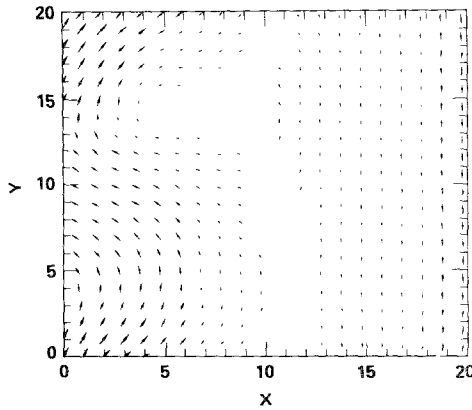


FIG. 4. The magnetic field resulting from the streamlined \mathbf{B} calculation procedure discussed in Section III.a.

arbitrarily chosen $B_y(X = X_{\min}) = 2 + \cos(\pi Y)$ and $B_y(X = X_{\max}) = -2$ as the boundary conditions for this test case. Consistent with this choice to ensure $\nabla \cdot \mathbf{B} = 0$, we are required to set $\partial B_x / \partial x(X = X_{\min}) = \pi \sin(\pi Y)$ and $\partial B_x / \partial x(X = X_{\max}) = 0$.

The numerical procedure discussed in Section III.a for Eq. (10) has been applied to this example. The resulting test magnetic field vectors are shown in Fig. 4. The real test is now whether the original J_z can be recovered by taking the curl of the magnetic field. The result of this numerical curl operation is shown in Fig. 5. Note that the scale factors for the minimum and maximum contours (shown on the upper left and right corners of the plots, respectively) are not the same as the input J_z in Fig. 2. This is due to the additive constant required in J_z so that the resulting \mathbf{B} field is consistent with the imposed boundary conditions. This constant is roughly

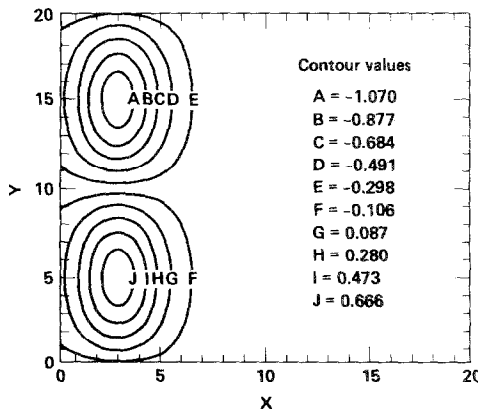


FIG. 5. Recovery of J_z from the curl of \mathbf{B} shown in Fig. 3. Note that the minimum and maximum contour values (in the upper left and right corners, respectively) differ from those of the initial J_z by only 3% after an additive constant of -0.202 is taken into account.

-0.202. After subtracting this constant, the new J_z differs from the original by less than 3%, which is consistent with the truncation of our second-order algorithms on the test mesh. Finally, the largest $\nabla \cdot \mathbf{B} < 2 \times 10^{-3}$.

The \mathbf{B} test proves that given an arbitrary plasma source J_z and consistent externally imposed boundary conditions, the correct \mathbf{B} is obtained and it has acceptably small divergence.

E Tests

The streamlined Darwin \mathbf{E}_t calculation can be tested in much the same manner as used in the \mathbf{B} tests. We find the task of decomposing \mathbf{J} so troublesome with general boundary conditions that the question of how well the standard approach works is not considered. Thus, we present only the results of the test cases proving that the new iteration procedure works well.

To demonstrate the streamlined \mathbf{E}_t technique, we need to verify that we can solve Eq. (21) and then extract the correct \mathbf{E}_t . To carry out this test, we proceed in the following manner. First, we begin with a known \mathbf{E}_t , which is used to form the right-hand side of Eq. (22). This known \mathbf{E}_t is obtained from a divergence-clean of an arbitrary vector \mathbf{E} . We also choose an arbitrary μ . The right-hand side of Eq. (22) is constructed by noting that it is equal to $\nabla^2 \mathbf{E}_t - \mu \mathbf{E}_t$ and can be constructed, therefore, from the chosen quantities. The boundary conditions are that \mathbf{E}_t tangential is zero at X_{\min} and X_{\max} . Finally, we reconstruct \mathbf{E}_t using these derived sources with the steps elucidated in Section III.b.

We start by assuming an arbitrary \mathbf{E} with components in the $x - y$ plane. We use the form

$$\mathbf{E}(i, j) = \exp\{-[X(i) - a]^2/5\} \cos[\pi Y(j)/10][\hat{\mathbf{e}}_x - \hat{\mathbf{e}}_y]. \quad (30)$$

We also choose an expression for μ ; here we use

$$\mu(i, j) = 2[X(i)/20 + 1 - \cos[\pi Y(j)/5]]. \quad (31)$$

The original \mathbf{E} , Eq. (30), is shown in Fig. 6; the decomposed \mathbf{E}_t is shown in Fig. 7; and μ , given by Eq. (31), is shown in Fig. 8. Following the test procedure outlined above, we applied the iteration for \mathbf{E}_t given in Section III.b. In five iterations, the first residue of Eq. (23)

$$\text{First Residue} = \nabla^2 \psi^n + \nabla \cdot \xi^{n+1} \quad (32)$$

in step (3) is $317. \times 10^{-4}$; in ten iterations it is 85.1×10^{-4} and drops further to 15.7×10^{-4} after 20 iterations. If an over-relaxation factor of 1.4 is used in generating the next iterate for ψ , the first residues ($150. \times 10^{-4}$, 32.6×10^{-4} , and 4.4×10^{-4} , respectively) show more rapid convergence.

After 20 iterations, the scalar function ψ required to extract \mathbf{E}_t from ξ in step (5) is shown by contour plot in Fig. 9. The \mathbf{E}_t that results from this process is shown by

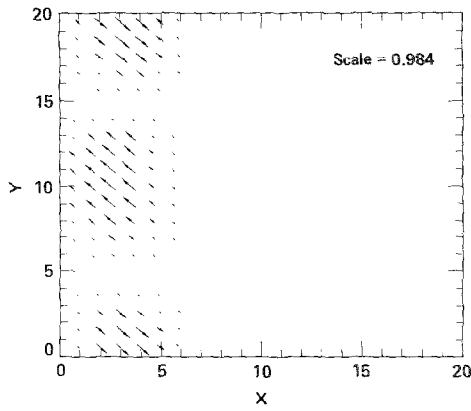


FIG. 6. Total E field selected for a test of the E_r procedure.

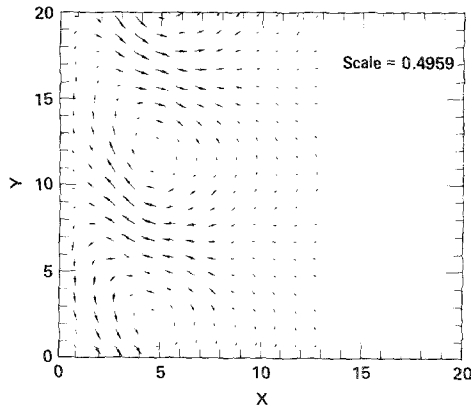


FIG. 7. Decomposed E_r field obtained from E in Fig. 6.

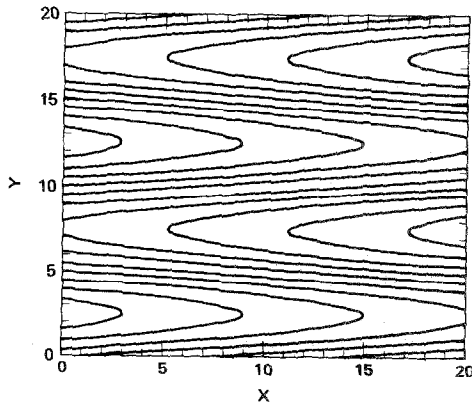


FIG. 8. Test μ factor for the new Darwin E_r calculation test.

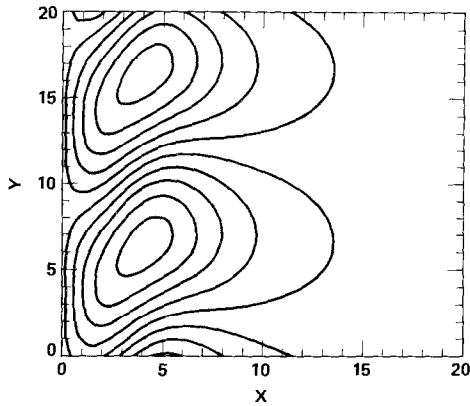


FIG. 9. The scalar ψ that is needed to extract \mathbf{E}_t from ξ in the final step of the streamlined \mathbf{E}_t calculation of Section III.b.

vector plot in Fig. 10. Note in comparing the scale factors of Figs. 7 and 10 that vectors agree to nearly three significant figures.

This is a rather stringent test of the streamlined algorithm because of the sharp gradients in the μ test function. In typical previous Darwin applications, comparisons were made between runs with, for example, three and five overall iterations. If the simulated physics remained invariant, the assumption was made that the \mathbf{E}_t iteration was "converged." Our calculation will work at least as effectively for this type of test. When the \mathbf{E}_t calculation must satisfy more stringent requirements and, especially, for more complex boundary condition arrangements, our new procedure has the advantage.

Finally, the number of overall iterations generally will decrease if we keep ψ for the first guess on the next time-step. Many iterations are required to generate the

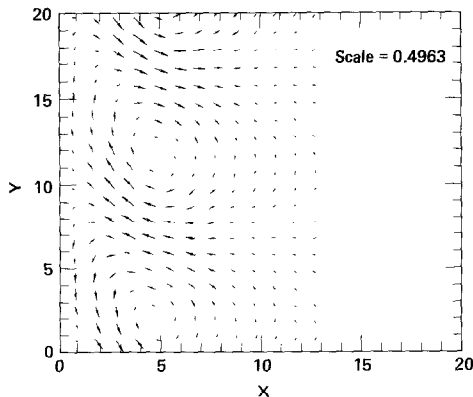


FIG. 10. Recovered \mathbf{E}_t to be compared with the input in Fig. 7. Note that the vector scale factor in the upper right agrees to three significant figures with the scale factor of the input \mathbf{E}_t given in Fig. 7.

long scale-length character of ψ , and this characteristic of ψ changes more slowly with time than short wavelength phenomena.

V. SUMMARY AND CONCLUSIONS

We have found a new streamlined method of implementing the Darwin model that greatly facilitates its use in nonneutral plasmas with nearby boundaries. Specifically, we have eliminated the need to decompose several plasma-derived source terms so that boundary conditions required for this purpose are no longer needed. We have tested the new methods and have verified that they work on simple test cases. We are now implementing this new procedure in cylindrical geometry with the ultimate application to accelerator physics.

ACKNOWLEDGMENTS

The authors wish to thank Drs. David S. Kershaw and Manoj K. Prasad for useful discussions. This work was performed under the auspices of the U.S. Department of Energy by the Lawrence Livermore National Laboratory under Contract W-7405-Eng-48.

REFERENCES

1. A. N. KAUFMAN AND P. S. ROSTLER, *Phys. Fluids* **14** (1971), 446.
2. C. W. NIELSON AND H. R. LEWIS, *Methods in Computational Physics* (Academic Press, New York, 1976), Vol. 16, pp. 367-388.
3. J. BUSNARDO-NETO, P. L. PRITCHETT, A. T. LIN, AND J. M. DAWSON, *J. Comput. Phys.* **23** (1977), 300.
4. D. W. HEWETT AND C. W. NIELSON, *J. Comput. Phys.* **29** (1978), 219.
5. D. W. HEWETT, *Space Sci. Rev.* **42** (1985), 29.
6. R. D. RICHTMEYER AND K. W. MORTON, *Difference Methods for Initial-Value Problems* (Interscience, New York, 1976).
7. J. K. BOYD AND D. W. HEWETT, *Bull. Amer. Phys. Soc.* **29** (1984), No. 8, 1436.